Journal of Physics: Conference Series

PAPER • **OPEN ACCESS**

Multivariate Image Analysis for Core Monitoring in PWRs

To cite this article: Mohamed Y.M. Mohsen *et al* 2023 *J. Phys.: Conf. Ser.* **2616** 012059

Multivariate Image Analysis for Core Monitoring in PWRs

Mohamed Y.M. Mohsen[1] , Tarek F. Nagla[2] , Mohamed Elsamahy[3] , Mohamed A.E. Abdel-Rahman[1]
[1] Military Technical College, Nuclear Engineering Department, Cairo, Egypt.
[2] Nuclear Engineering Department, Faculty of Eng., Alex. University, Alex., Egypt.
[3] University of Saskatchewan, Saskatoon, SK, Canada.

E-mail: moh39333@mtc.edu.eg

Abstract. In pressurized water reactor (PWR) it is crucial for the operator to monitor the reactor parameters at the same time, such as temperature, pressure, boron concentration, control rod position, coolant density, etc., in order to make proper decision. However, the huge size of data reading from the different instrumentations, in addition to the limited human ability to visually detect, interpret, assess add a lot of uncertainty to the operator qualitative and quantitative analysis of the reactor performance. Therefore, this paper proposes the utilization of radial thermal flux maps (Neutron Images) technique, positioned on the reactor core as a sensitive monitoring technique for all changes of the reactor parameters as a result of the position of the control rods changing. Hence, the features contained in these neutron images are extracted (Multivariate image analysis and regression) via Principal Component Analysis (PCA), and Cluster Analysis (Dendrogram). To determine the effectiveness of the suggested technique in determining the location of the control-rods, several simulations are run. The 3D TRITON FORTRAN-code was utilized to simulate the radial thermal neutron flux of the Westinghouse 2775-MWth PWR benchmark at 100% thermal power generation. The SIMCA software programme is used to develop, test, and generalise the PCA model. Additionally, clustering analysis (CA) is carried out using the statistics software programme Minitab in order to demonstrate the effectiveness of the suggested method.

Keywords: Chemometrics; Control rod position; PCA, Neutron Flux, Neutron Image, Dendrogram.

1. Introduction

In order to change the status of a PWR (start the reactor, increase its power level, reduce it power levels or shut-down) operators follow a certain prepared sequence of steps [1]. Each step of this sequence contains the position of a group of control-rods at the start and at the end of the same step. The control-rods in during a certain step should move to the appropriate position prior to the start of the following step. The change of the control-rods position impacts the neutron reaction rate. The rod movement sequence is set to maintain the reactor within safe operating limits. It is vital that the operator follow the sequence to ensure safe reactor operation and good fuel management. Threedimensional (3-D) modelling of the reactor core is necessary for the simulation of nuclear power plant safety circumstances [2] such as TRITON code [3] to ensure that the control-rods' insertion reactivity for a PWR is physically accurate described.

2. Simulation of PWR reactors

2.1. Simulation procedures

The same procedure in presented [4] to develop the 3D numerical benchmark of the reactor core is also depicted during the investigations of this paper. Whereas the benchmark computation done using a common polynomial fitting in the cross-section modelling of the core, the TRITON code was used to describe the reactor-power transient is given material-dependent, few-group cross sections that are functions of both the instantaneous T-H conditions and the explicit control rod motion. Two cross-section libraries are used to improve calculation accuracy. one for fully rodded fuel compositions and the other fully unrodded. Each composition is described by material properties (due to changes in the fuel design) and burn-up. By choosing an appropriate range for the independent variables, the three conditions for the burn-up can be achieved. Specifically, component vector accounting for history of burnable poison (BP), spectral history (Tmod), and exposure (GWD/t). In addition, the thermal-hydraulic code [2] includes three-dimensional six-equation, two-phase fluid model coolant conditions and the code can treat a non-condensable gas in a vapor field and dissolved solute in the liquid field, where the T-H conditions connected to the time-step are used to derive fluid state dependent material characteristics and heat transfer coefficients. If the reactivity insertion is significant enough, the reactor may briefly reach prompt criticality, which could then result in fuel rod damage and localized Departure from Nucleate Boiling (DNB). Because every neutronic node is immediately related to a thermal-hydraulic cell and a heat structure, the Cartesian geometry vessel model geometrically fits the neutronic core model precisely. The neutronic model is created using three-dimensional Cartesian geometry. There are 205 levels of zplanes axially, which reflect various assembly compositions. 36 x-planes and 36 y-planes are employed in the radial plane. Modeled neutron groups include two prompt and six delayed. (3.213e-12 W-s/fission) and (3.206 e-12 W-s/fission) are the energy releases per fission in the prompt groups.

2.2. PWR understudy

The same PWR presented in [4] is also investigated during this paper. It is a three-loop PWR. The hot full power (HFP) condition of the reactor is described as 2770 MWth (900 MWe net), Groups 1-6 of control rods are fully removed, average fuel and moderator temperatures are 618.3 0 C and 306.6 0 C, respectively. The core model is composed of 64 radial nodes that correspond to the reflector and 157 nodes in the radial plane that represent one fuel assembly apiece. The entire core height is made up of upper and lower reactors, each measuring 30.0 cm, and 16 axial layers with heights of 7.7, 11.0, 15.0, 30.0 (10 layers), 12.8 (two layers), and 8.0 cm. The core is often represented by (265680) neutronic mesh points. Eleven distinct neutronic cross section sets each represent a different component of the core's material makeup. Microscopic cross sections for transport, scattering, absorption, and fission as well as their derivatives with respect to boron density, moderator temperature, moderator density, and fuel temperature are all calculated using fourth-order polynomial fitting. The start of the first cycle without any xenon or iodine poisoning or fuel depletion is used to depict the operational circumstances of a reactor. The fuel receives 98.1 percent of the thermal energy, and the coolant receives the remaining 1.9 percent. The channels are evenly dispersed among the coolant's mass flow. Analytical dependence was used to depict UO2's thermal conductivity.

$$\lambda(UO2) = 1.05+2150. (T-73.15) \quad (1)$$

The original model for uranium dioxide's heat capacity was maintained. The thermal conductivity of zircaloy was expressed via a three-term polynomial that is simpler. The linear representation of zircaloy's heat capacity was

$$Cp\ (ZIRCA) = 252.54+0.11474\times T \quad (2)$$

The Doppler temperature formula is TD = 0.3×TFC + 0.7 ×TFS (3) with TFC and TFS standing for, respectively, the fuel rod center and surface temperatures. The obtained steady state and transient results were found to be unaffected by the aforementioned adjustments. In this work, the location of the control rods is used to generate images of the reactor core (group-D insertion). More specifically, four case-studies are considered: control-rods are completely out of core, control-rods are inserted at 1/4 core, 1/2 core, 3/4 core, the control rods are finally fully placed into the core. Due to the change in control-rods' position the change in the Boron concentration, Moderator temperature, Density of coolant are determined hence, the thermal neutron flux relative to these changes is also calculated. It is worth highlighting, the thermal neutron flux relative to each controlrods position is captured at the top of the core surface as shown in Figure (1).

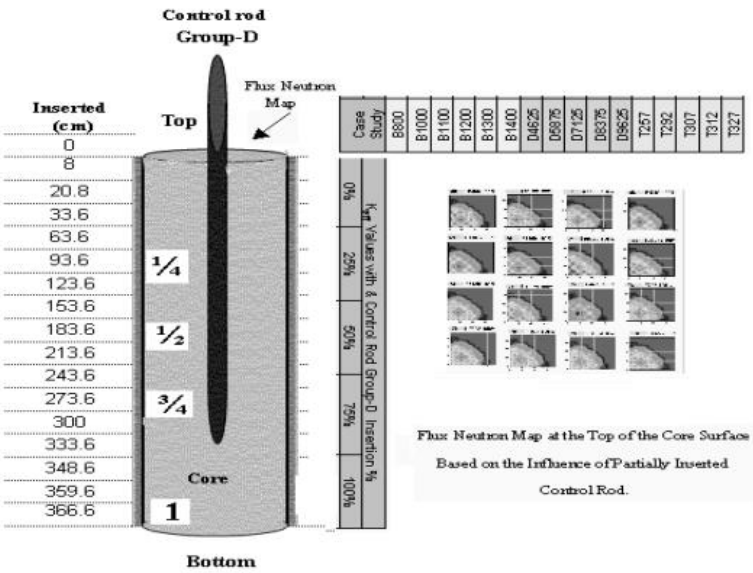

Figure 1. diagram for the control-rods position and it's corresponding the thermal neutron flux images.

Figure (2-a) shows the thermal neutron flux map (36×36) pixel at the top of the core surface in case of group control rod which are fully withdrawn position, Boron Concentration=1200.2 ppm, moderator temperature =306.6 0C, water Density = 0.7125 (g/cm3) at 100% power. While, Figure (2-b) shows the same case study before except the group-D control rod a fully insertion.

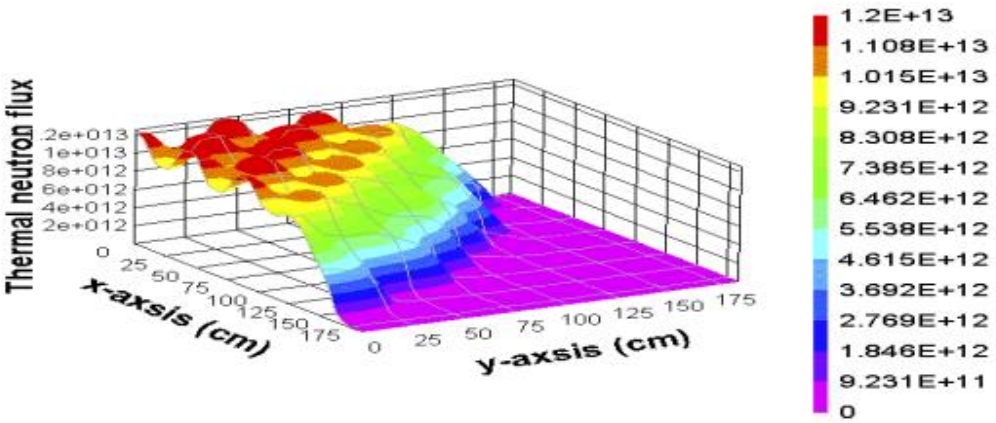

(a)

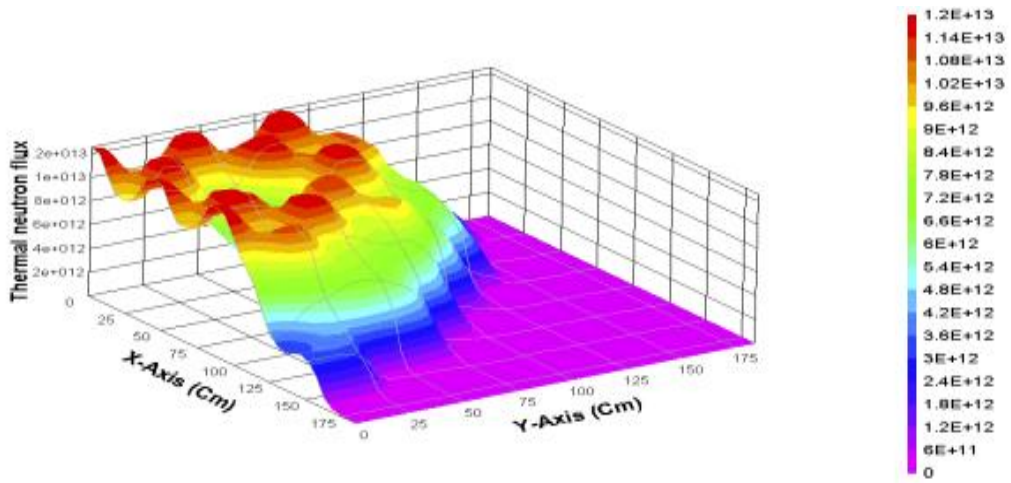

(b)

Figure 2. 3D presentation of the spectral footprint of the control-rods inside the thermal neutron flux: (a) at 0cm, (b) at 366.6cm.

The summary of the change in previous work is presented in Table 1, which shows the effective multiplication factor (Keff) values with changes in movement of the control rod Group-D. Table (2) manages this data by adding the number of observations to each case study. The neutron flux map (neutron image) that resulted from this study by using the TRITON code is shown in figure 3.

Table (1) The effective multiplication factor (Keff) values with change control rod position

Case Study	**Article I. K_{eff} Values with & Control Rod Group-D Insertion %**				
	0%	**25%**	**50%**	**75%**	**100%**
Article II. B800	1.0406101	1.0393746	1.0352499	1.262512	1.0230817
B1000	1.0196996	1.018526	1.0145719	1.00609	1.0031898
B1100	1.007826	1.0066775	1.0027939	0.99452841	0.99172378
B1200	0.99958658	0.99846756	0.99466133	0.198668826	0.98404187
B1300	0.98980314	0.98871768	0.98498774	0.97726595	0.97473848
B1400	0.98020881	0.97914147	0.97550505	0.96802974	0.96560699
D4625	0.92759943	0.92626816	0.92154396	0.91303498	0.91057402
D5875	0.97078055	0.96954471	0.96521389	0.95665359	0.95392674
D7125	0.99958658	0.99846756	0.99466133	0.198668826	0.98404187
D8375	1.0195789	0.99846756	1.015311	1.0082245	1.0058501
D9625	1.0339944	1.0185966	1.0303279	1.0242522	1.0222781
T257	1.0009763	0.99986404	0.99606806	0.9881047	0.98547071
T292	0.9999311	0.9987013	0.99486709	0.98680806	0.98439902
T307	0.99958658	0.99846756	0.99466133	0.198668826	0.98404187
T312	0.99944288	0.9983235	0.99451387	0.98654985	0.98388976
T327	0.99900407	0.99789119	0.99407941	0.98610383	0.98344994

Table (2) The Addition of the No. of observation to each case study

No.	Case study	No.	Case study	No.	Case study	No.	Case study	No.	Case study
1	B800-0%	17	B800-25%	33	B800-50%	49	B800-75%	65	B800-100%
2	B1000-0%	18	b1000-25%	34	B1000-50%	50	b1000-75%	66	b1000-100%
3	B-1100-0%	19	B-1100-25%	35	B-1100-50%	51	B-1100-75%	67	B-1100-100%
4	B1200-0%	20	B1200-25%	36	B1200-50%	52	B1200-75%	68	B1200-100%
5	B1300-0%	21	B1300-25%	37	B1300-50%	53	B1300-75%	69	B1300-100%
6	B1400-0%	22	B1400-25%	38	B1400-50%	54	B1400-75%	70	B1400-100%
7	D4625-0%	23	D4625-25%	39	D4625-50%	55	D4625-75%	71	D9625-100%
8	D5875-0%	24	D5875-25%	40	D5875-50%	56	D5875-75%	72	D5875-100%
9	D7125-0%	25	D7125-25%	41	D7125-50%	57	D7125-75%	73	D7125-100%
10	D8375-0%	26	D8375-25%	42	D8375-50%	58	D8375-75%	74	D8375-100%
11	D9625-0%	27	D9625-25%	43	D9625-50%	59	D9625-75%	75	D4625-100%
12	T257-0%	28	T257-25%	44	T257-50%	60	T257-75%	76	T257-100%
13	T292-0%	29	T292-25%	45	T292-50%	61	T292-75%	77	T292-100%
14	T307-0%	30	T307-25%	46	T307-50%	62	T307-75%	78	T307-100%
15	T312-0%	31	T312-25%	47	T312-50%	63	T312-75%	79	T312-100%
16	T327-0%	32	T327-25%	48	T327-50%	64	T327-75%	80	T327-100%

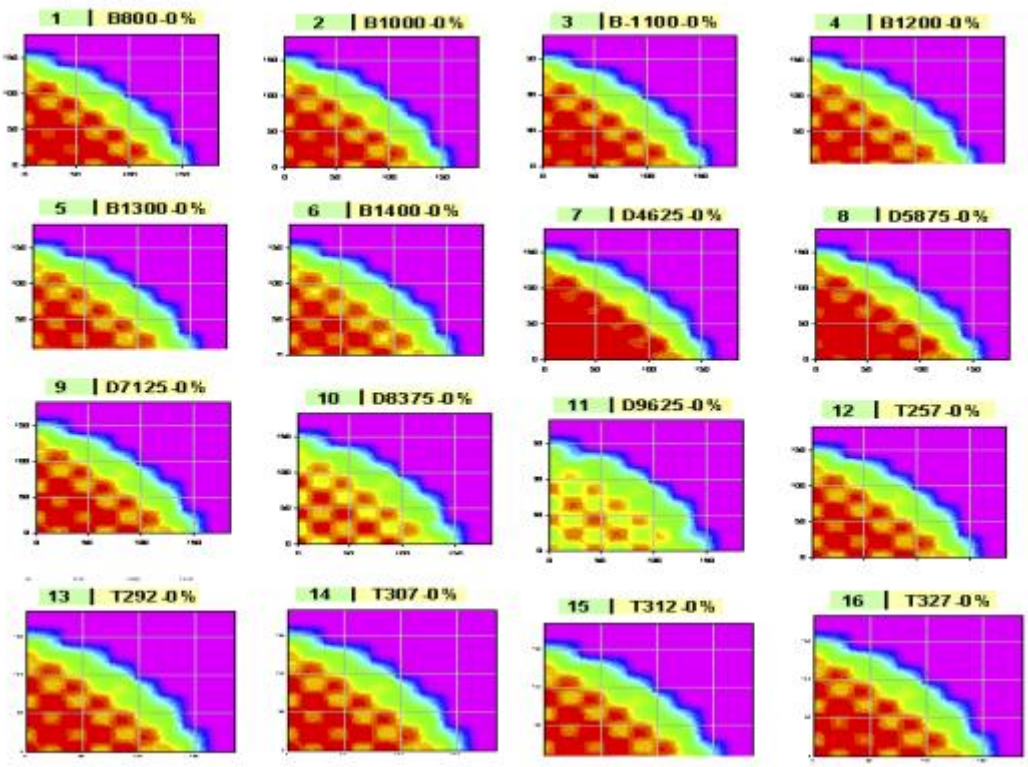

Figure 3-a. shows the neutron flux map (Neutron Image) for the case study from 1-16.

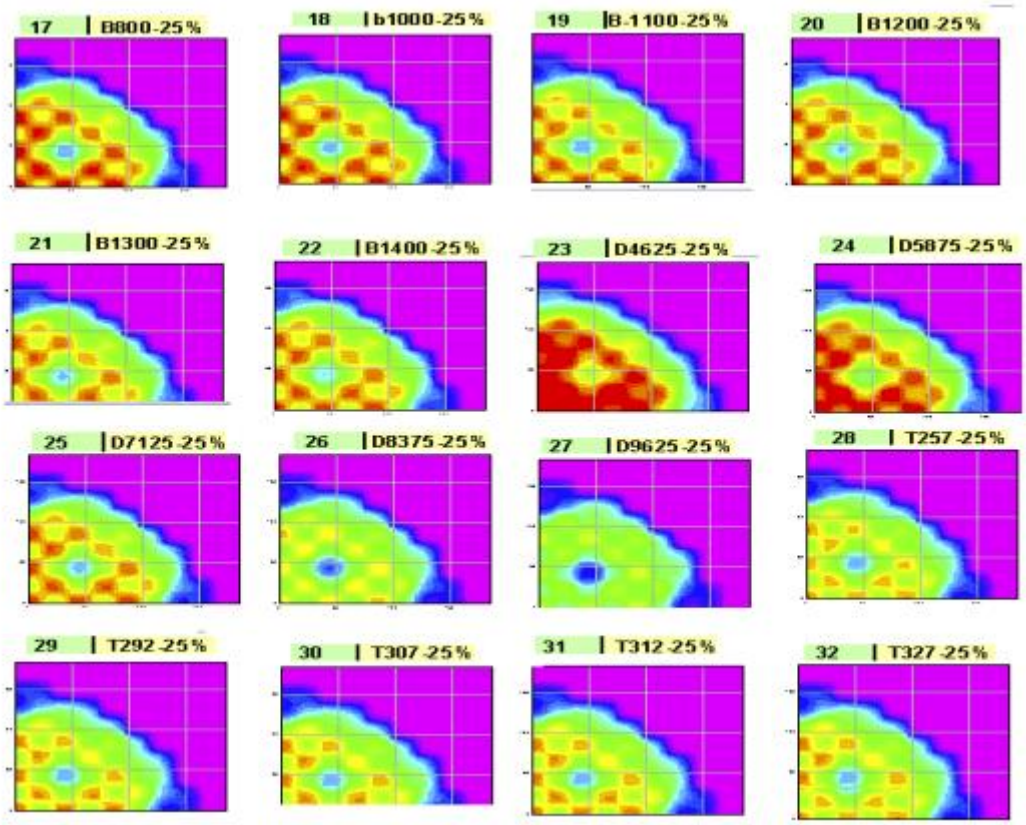

Figure 3-b. shows the neutron flux map (Neutron Image) for the case study from 17-32.

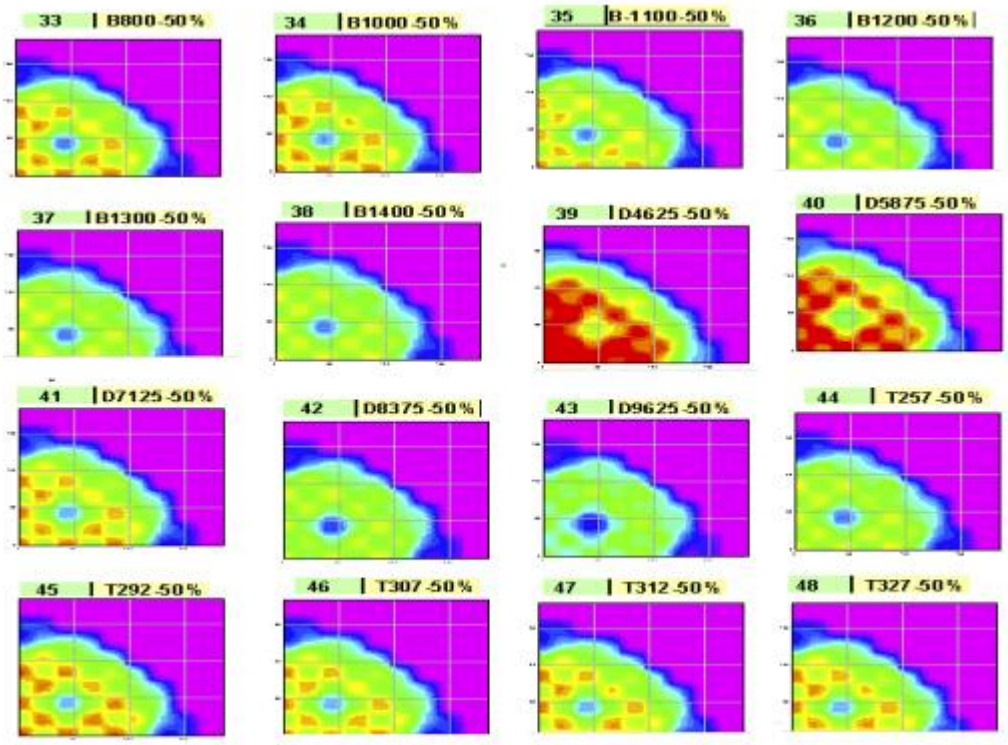

Figure 3-c. shows the neutron flux map (Neutron Image) for the case study from 17-32.

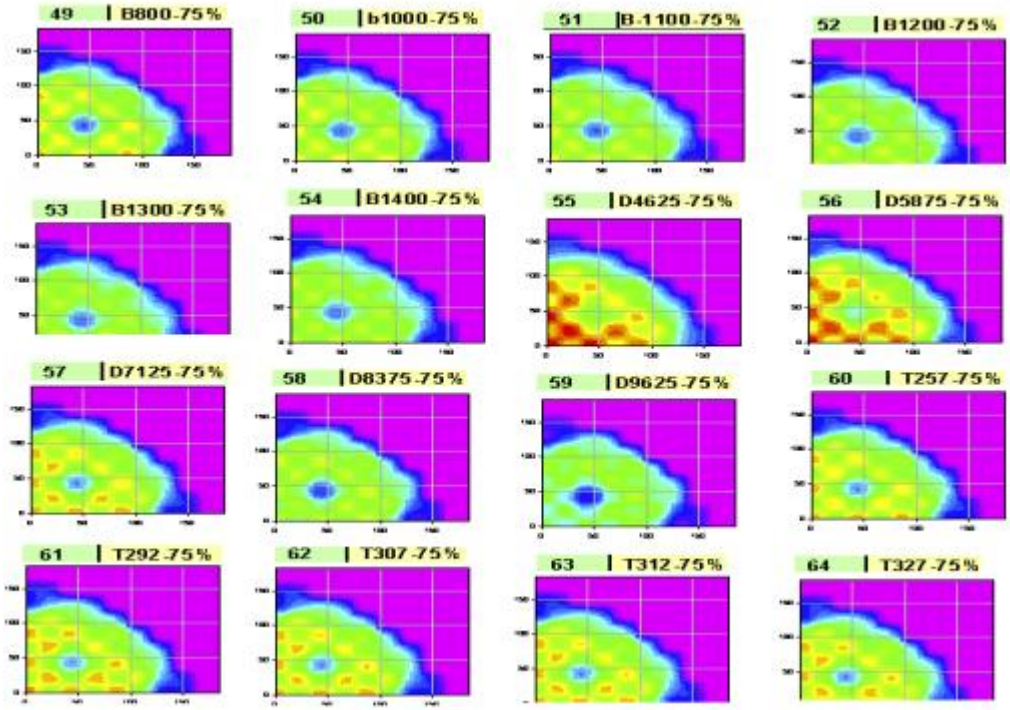

Figure 3-d. shows the neutron flux map (Neutron Image) for the case study from 49-64.

3. Multivariate analysis

Multivariate data analysis methods have gained popularity over the past ten years and are now employed in practically all areas of scientific research [5, 6]. This is because many scientific investigations call for the simultaneous study of relationships between three or more variables. In addition, the development of freely available and user-friendly software packages for carrying out multivariate analyses, along with the introduction of high-speed computers with vast storage capacities the use of multivariate approaches draws focus away from univariate and bivariate examination of the mean and variance of a single variable. In addition to the study of the covariance or correlations, which show the strength of the relationship among three or more variables, there is also the pairwise relationship between two variables. PCA and cluster analysis dendrogram are the multivariate data analysis methods used in this study.

3.1. Principle Component Analysis (PCA)

Today, measurements are getting easier and easier to perform as apparatus becomes more complex. Numerous characteristics that describe the samples can be gathered for image analysis and process control. Finding a solution for coping with thus many, often associated variables is the main challenge. Due to the possibility of correlation, the conventional method of taking each variable into account separately may produce inaccurate conclusions in such circumstances and may even be impractical. Because there are so many factors that need to be monitored. Finding a system's underlying structure and simplifying its description are frequent goals of data analysis. The variation in the data is captured in a few main components, or latent variables, that are orthogonal to one another using Principal Component Analysis (PCA) [7]. As a result, there are opportunities to identify patterns and trends in the data and to determine which variables significantly influence the patterns and trends. PCA can be used to monitor the dynamics of a process and, as a result, spot process disruptions early on. The variables that are causing the disturbances can then be found and fixed.

3.2. Cluster Analysis (Dendrogram)

When it is desired to identify groupings of related items that can be regarded as belonging to a "category," cluster analysis algorithms are used in unsupervised pattern recognition [8]. Additionally, clustering can be used with variables to identify collections of related variables, typically with the goal of choosing the right variables for calibration methods. Visual approaches, Hierarchical methods (Agglomerative and Divisive), and Non-hierarchical methods are the three categories under which clustering techniques [9] have been classified. The observation of main component plots serves as the foundation for many visual approaches. The most widely used method among the others is hierarchical agglomerative method. The grouping is shown graphically on a dendrogram. Usually, it is drawn in reverse, beginning with the final cluster of all the objects and with similarity.

4. Principle of CCD –Neutron Camera

To see the internal structure of macroscale samples, use radiography. It is based on the idea that radiation weakens as it travels through matter, depending on the sample's geometry and material [10]. Neutron radiography offers an essential validation to radiographic examinations in the field of nondestructive testing (NDT), in addition to the well-known radiographic examinations with x-rays and - rays. [11] Neutrons are absorbed by some light materials, such as hydrogen, boron, and lithium, in contrast to x-rays, yet they pass through many heavier materials [12]. In addition to being a significant instrument for the analysis of radioactive materials, neutrons may even discriminate between various isotopes. The detector is one of the most important elements of a radiography facility. It typically consists of a two-dimensional integrated imaging equipment. A CCD-based neutron radiography detector has been developed for applications needing high quantitative precision as well as for neutron tomography studies. It is made up of a neutron-sensitive scintillator screen, a nitrogen-cooled slowscan CCD camera, and a mirror that directs the scintillator's light toward the CCD camera [13-15]. The entire assembly is enclosed in a thin, airtight shell. A CCD-camera based neutron sensitive detector system has been created in accordance with these specifications, as illustrated in Figure (4) [13]. Its detection system operates in the following manner: After passing through the sample, the neutron beam arrives at the neutron sensitive scintillator screen. In order to prevent the camera from being in the direct neutron beam, which would harm the chip, the light emitted from the screen is mirrored to the camera by a mirror and focused on the CCD-chip by a lens. Together with shielding components, these parts are housed in a light-shielded tube to shield the CCD camera from neutron and beta radiation. In order to read out the data recorded on the CCD chip, reconstruct, and process the digitized picture data obtained with this imaging equipment; the CCD camera is connected to a computer.

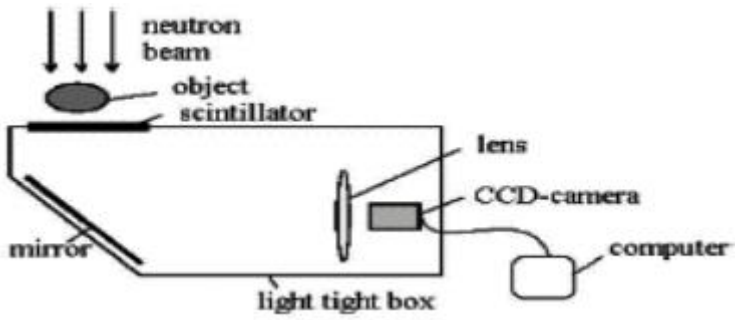

Figure 4. shows the principle of a CCD –neutron radiography detector.

5. Analysis of Neutron Flux Images

After collecting the 80 data observations, the PCA method is applied. It can be observed form Figure (5) that the first two PCA components are enough to represent a good model for the scatter scores plot. In addition, it can also be observed that the 80 case-studies are classified to five clusters. Where, first cluster is in the right top region represent the case study 100% full insertion control rod inside the core. The second cluster in the right bottom region represents the case study 0% full insertion control rod outside the core. The third cluster and the fourth cluster nested in the central region represent the case study 25% insertion control rod inside the core and represent the case study 75% insertion control rod inside the core respectively, because the power is consistent at 100 % full power. The last cluster in the left central region represent the case study 50% insertion control rod inside the core and also that case study D4625-100% is an outlier. The dendrogram shown in Figure (6) shows that the similarities and differences among the 80 case studies. To shield the CCD camera from neutron and gamma radiation, these components are housed in a light-shielded tube with shielding components. The CCD camera is connected to a computer in order to read out the data recorded on the CCD chip, reconstruct, and process the digitized image data produced with this imaging device. This indicates the robustness of the prediction of the proposed technique. The observations No.71 (D9625-100%) represent the water density 0.9625 (g/cm3) at 100% full insertion control rod outlier for all data set 80 observations and N0.75 (D4625-100%) represent the water density 0.4625 (g/cm3) at 100% full insertion control rod outlier for data set represent only 16 case studies for 100% full insertion control rod. It is clear that the 5th cluster from the left direction 0%, 100%, 25% nested with 75% and the last 50%. It was proved that pattern recognition by using the multivariate methods such as PCA and CA [16-18] is more visual, faster and easier.

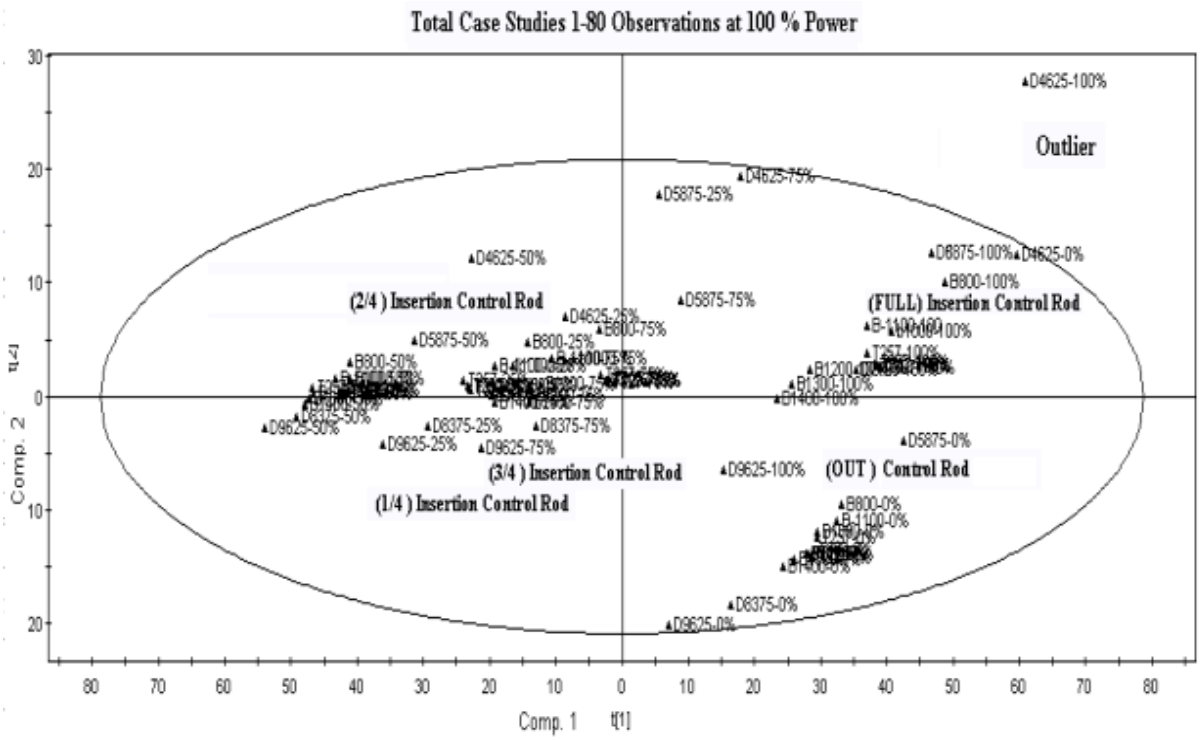

Figure 5. The score scatter plot of the PCA analysis including the 80 observations

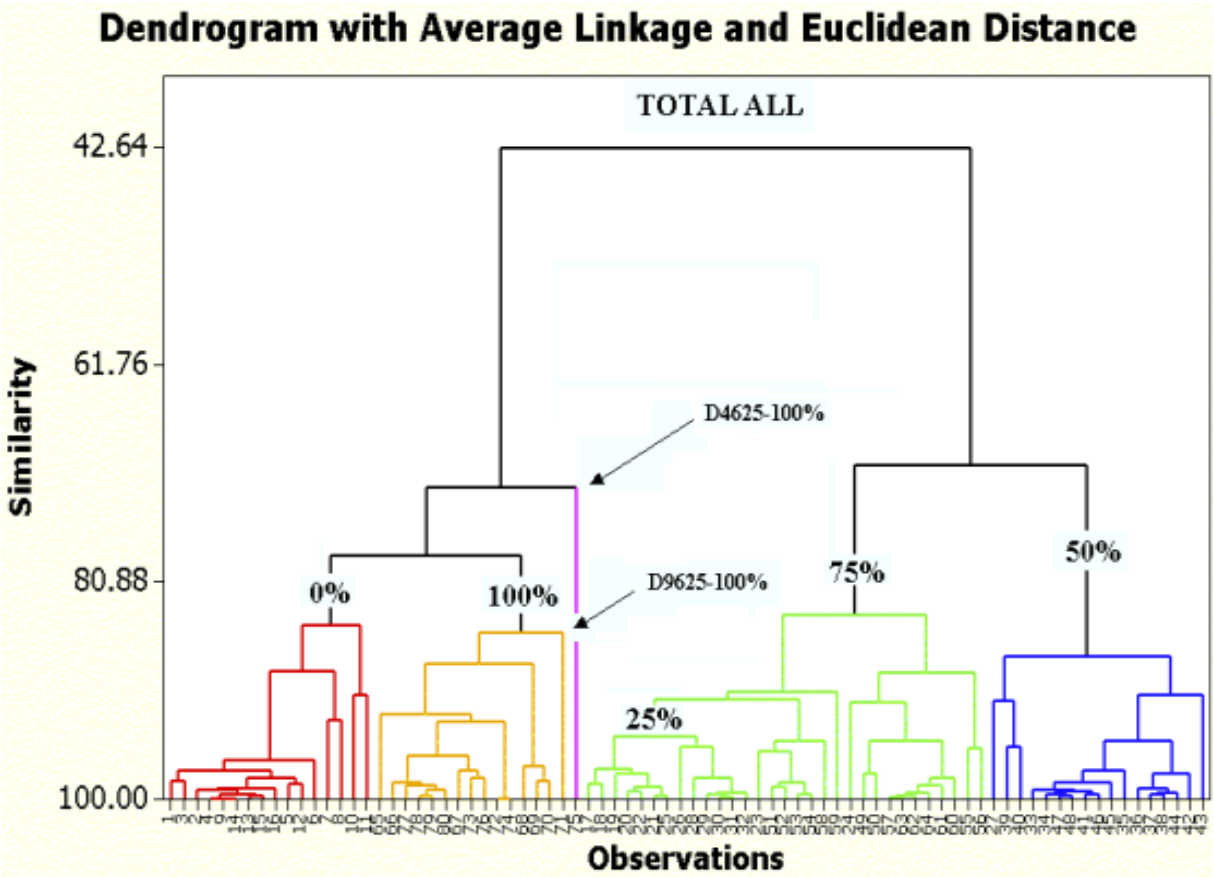

Figure 6. Hierarchical Cluster Analysis on 80 observations – Dendrogram.

6. Conclusion

In this study, investigations were conducted to determine whether it could be possible to identify PWR control-rod positions by analyzing neutron flux photographs. In this case, the detection of the change in the control-rod locations under a condition of full thermal power operation was accomplished using principal component analysis (PCA). The findings of these investigations have demonstrated the effectiveness of the suggested technique because it was able to successfully overcome any data size restrictions as well as restrictions imposed by outlier samples, extract noise, and analyse all variables simultaneously with further assurance of performance efficiency. It is worth mentioning, that applying changes in the reactor operating conditions, such as different Boron concentrations, moderator temperatures and coolant densities, dictate the adaptability of the proposed technique in order to maintain the performance efficiency. This is, however, is the subject of the authors' current research. The Authors also suggest the implementation of the proposed technique in real time using on-line neutron cameras (CCD) and computers. The results of the suggested research areas will be reported in a subsequent publication.

References

[1] Elsamahy M *et al* 2021 Continuous online monitoring in pressurized water reactors during flexible operation using PLSR-based technique. *Ann. Nucl. Energy*, vol. **161**, p. **108473**.
[2] Mohsen M *et al* 2020 Thermal-hydraulic and solid mechanics safety analysis for VVER-1000 reactor using analytical and CFD approaches. *Prog. Nucl. Energy*, vol. **130**, p. **103568**.

[3] Daneri A *et al* 1968 TRITON: A MULTI-GROUP DIFFUSION-DEPLETION PROGRAM IN THREE DIMENSIONS FOR IBM-360 *https://www.osti.gov/biblio/4600691*.
[4] Finnemann H et *al 1993* Results of LWR core transient benchmarks. *NEA*.
[5] Dillon W *et al 1984* Multivariate Analysis: Methods and Applications. *New York: John Wiley & Sons*.
[6] Roggo Y *et al* 2005 Infrared hyperspectral imaging for qualitative analysis of pharmaceutical solid forms *Analytica Chimica Acta*, vol. **535**, pp. **79-87**.
[7] Jackson J 2005 User's Guide to Principal Components. *New York: John Wiley & Sons*.
[8] Elsamahy M *et al* 2021 Pattern Recognition–Based Technique for Control Rod Position Identification in Pressurized Water Reactors *Nucl. Technol*, vol. **207**, pp. **558-574**.
[9] Massart D and Kaufman L 1983 The Interpretation of Analytical Chemical Data by the Use of Cluster Analysis. *New York: John Wiley & Sons.*
[10] Abdel-Rahman M *et al* 2019 Study of γ-Fast Neutron Attenuation and Mechanical Characteristics of Modified Concretes for Shielding and Sheltering Purposes. *Zeitschrift für anorganische und allgemeine Chemie*, vol. **645**, pp. **649-655**.
[11] Abdel-Rahman M *et al* 2019 Alpha spectroscopy and X-ray induced photocurrent studies of a SC CVD diamond detector fabricated with PLD contacts. *Radiat. Phys. Chem*, vol. **164**, p. **108357**.
[12] Abdel-Rahman M *et al* 2020 Penetrability of γ/n and Static Behavior of Newly Developed Concrete Using Different Passive Assay Techniques. *Nucl. Technol*, vol. **206**, pp. **766-778**.
[13] Koerner S *et al* 2000 Design and optimization of a CCD-neutron radiography detector. *NIM-A*, vol. **454**, pp. **158-164**.
[14] Martens H *et al* 2000 Sensory Analysis for Magnetic Resonance-image Analysis: Using Human Perception and Cognition to Segment and Assess the Interior of Potatoes, LWT - *J. Food Sci. Technol*, vol. **35**.
[15] Yu H and MacGregor F 2003 Multivariate image analysis and regression for prediction of coating content and distribution in the production of snack foods. *Chemometr Intell Lab Syst*, vol. **67**.
[16] Umetric AB 2005 SIMCA-P10.0 Tutorial. Umetri AB, Umeå.
[17] Minitab14.0 2005 *Enterprise Drive state college*.
[18] Groover P 2008 Automation, Production Systems, and Computer-integrated Manufacturing. *New Jersey: Prentice Hall Englewood Cliffs*.